Worldwide seismic observations of low frequency signals related to the 15 January 2022 Hunga-Tonga volcanic eruption

Jordi Diaz (jdiaz@geo3bcn.csic.es)
GEO3BCN-CSIC

Article

Keywords:

Posted Date: April 19th, 2022

DOI: https://doi.org/10.21203/rs.3.rs-1525341/v1

Version of Record: A version of this preprint was published at Communications Earth & Environment on November 16th, 2022. See the published version at https://doi.org/10.1038/s43247-022-00616-1.

Abstract

The eruption of the Hunga-Tonga volcano produced a high-energy explosion that was recorded globally by different scientific instruments, including broad-band seismometers. Seismic data recorded on global seismic networks is used to explore three main topics; the time evolution of the eruption, the atmospheric waves revolving around the Earth and the low-frequency, long-lasting signals recorded worldwide in the hours after the main event. From the inspection of the data we can assess that the eruption started on January 15 around 04:05 UTC, several minutes before the origin time reported in the seismic catalogs and included two large explosions at 05:30 and 08:35. As for the atmospheric waves, their energy was enough to be detected seismically during more than two complete circumambulations of the Earth, during a time span of three and a half days. The most notable seismic feature has been the low-frequency signals detected over several hours and interpreted as resulting from the excitation of Earth normal modes. To our knowledge, there are no previous examples of atmospheric-solid Earth coupling over such a long time interval and only two examples of normal mode excitation following volcanic eruptions, identified for the 1982 El Chinchón and the 1991 Mount Pinatubo eruptions.

1 Introduction

The Hunga-Tonga volcano, located in the South Pacific Ocean, began its recent activity on December 20, 2020 with multiple explosions and a high ash plume. After a period of relative calm, a powerful explosion devastated much of the island on January 14, 2022, followed on January 15 by the main eruptive event, which becomes one of the most powerful volcanic events recorded to date, with an energy release estimated between 4–18 megatons of TNT [1]. The eruption released material as high as 55–58 kilometers in altitude [2], producing the plume reaching 600 km in diameter, and generating, among other effects, a tsunami detected on the Pacific coasts, strong ionospheric disturbances(Themens et al. 2022) and a strong acoustic explosion in the atmosphere, which was heard but as far as the Alaska Peninsula, more than 9,700 kilometers away. Preliminary estimations attribute a VEI value of 5–6 to the eruption Yuen et al., (2022), Poli and Shapiro (2022). Using the time arrivals of body seismic waves at seismic stations around the world, the USGS earthquake center reported the location and origin time of the eruption, and assigned an equivalent magnitude of 5.8, corresponding to moderate size earthquakes.

The variation in atmospheric pressure generated by this explosion has spread throughout the planet, producing variations that have been detected by various types of sensors, from barometers integrated in weather stations to geodetic stations. This wave has been interpreted as a Lamb wave, a non-dispersive atmospheric wave with purely horizontal motion, which propagates at speeds close to 0.310 km/s, slightly slower than the speed of sound, and optimally transfer energy over large distances (e.g. Amores et al. 2022).

In this contribution we investigate the seismic signals generated by the Hunga-Tonga eruption recorded in global scale seismic networks, focusing on three key points; a description of the temporal evolution of the eruptive process derived from the analysis of seismic data, the seismic signals generated by the passage

of the atmospheric wave during its successive circumambulations around the Earth and the observation of low frequency signals during the hours following the eruption, interpreted as the result of the excitation of the Earth's normal modes due to the volcanic explosion. The first point will allow us to better define the evolution of the eruptive process, while the two others observations must be qualified as exceptional, since there are no previous references to worldwide seismic recordings of atmospheric disturbances for such an extensive period of time, withonly a couple of precedents, most recent 40 years ago, from normal mode excitation resulting from volcanic eruptions.

1 Temporal Evolution Of The Hunga-tonga Eruption

The USGS seismic catalog (https://earthquake.usgs.gov/earthquakes) reported the origin time for the Hunga-Tonga eruption at 04:14:45 and assigned an equivalent magnitude of 5.8, but the the closest station in our dataset (G.FUTU), located in the French overseas collectivity of Wallis and Futuna, at a distance of about 750 km from Hunga-Tonga, show a clear arrival at 04:02:35 (Fig. 1a, blue dashed lines), preceding the main phases arriving around 04:18, in the 0.01–0.04 frequency range. Similar arrivals can be detected at other seismic stations at distances ranging from 750 to 2480 km. This evidences that the eruption started around 15 minutes earlier than reported in the global seismic catalogs, that is, around 04:00 UTC. This is consistent with data derived from satellite images analysed byCarr et al., (2022) and Kumar Gupta et al. (2022), who reported that the eruption became visible just after 04:00 UTC. The difference with the origin time reported in the seismic catalogs seems to be related to by algorithms used for seismic detection, which analyse seismic signals with characteristic frequencies greater than 1 Hz. Although modeling will be necessary to explain the origin of the low-frequency waves preceding the main explosion, it is plausible to relate them to the movement of magma within the volcanic edifice. Their amplitude is much lower than that of the later phases, but the fact that they were recorded at distances greater than 750 km indicates that they are due to a process that involves a significant energy release.

The most energetic arrivals, consistent with the origin time reported in global seismic catalogs, show a complex waveform, with two energy packets with similar waveforms, separated by 200–210 s (Fig. 1a). This feature is consistently observed in stations located up to 2500 km from the volcano. A very similar double pulse, of lower amplitude, is observed around 05:30 UTC at the same stations (Fig. 1b, brown dashed lines). [7], reported that a lower-altitude umbrella cloud that becomes visible at the same time in the Himawari-8 geostationary satellite data. The similarity of the 04:00 and 08:30 signals, both made up of two discrete energy packets separated by about 200 s, suggests that they are related to similar processes. Yuen et al. 2022, have studied these arrivals using teleseismic P waves stacking, interpreting them as the result of 4 sub-events with similar waveforms, the last three forming the second energy packet described here. These authors interpret the similarity of waveforms as the effect of episodic eruptive activities with the same characteristics. We propose here a hypothesis interpreting that the first energy packet corresponds to a volcanic explosion, while the second corresponds to the reflection of the atmospheric waves generated by this explosion in an atmospheric discontinuity, as the upper limit of the stratosphere.

The more complex waveform observed in the second packet would not be the result of multiple sub-events, but of multipathing effects on the reflected signal. The validity or not of this hypothesis must be analyzed by carrying out propagation models in the atmosphere.

From the inspection of the January 15 seismic records in stations distributed all over the planet, a third highly energetic signal can be identified around 08:35, approximately 4 and a half hours after the main event. As seen in Fig. 1c, the move-out and the decrease in amplitude of this signal is similar to those of main signal, suggesting that they share the same source area. Carr et al., (2022), analysing data from the GOES-17 satellite, reported that an overshooting plume core reached the upper stratosphere at 08:41. Satellite data analysed by(Kumar Gupta et al. (2022) have also shown a plume overshoot between 08:10 and 08:30 UTC. These plumes clearly appear to be the result of the seismically detected explosion. The Hunga-Tonga event around 8:35 UTC has not been included in seismic catalogs, probably because the algorithms used for event detection are not sensitive to its frequency content. However, the signal can be detected all over the world, suggesting that its equivalent magnitude should be in the range of 5-5.5. Therefore, we can state that during the first hours of the Hunga-Tonga eruptive process there were three large explosions detected seismically. At least the main event, with origin time around 04:00 UTC and the event at 8:35 were detected worldwide, suggesting equivalent magnitudes greater than 5.0. The event at 05:30 UTC is difficult to identify at distant seismic stations as the first arrival overlaps with the coda of the main event.

2 Seismic Recording Of The Atmospheric Wave

The Hunga-Tonga eruption generated an atmospheric Lamb wave detected throughout the world by different types of sensors, including broadband seismic stations. Figure 1b shows the signal induced by the passage of this wave, which here appears as a high-amplitude, low-frequency signal with a duration greater than one hour. As Lamb waves propagate with a speed close to 310 m/s, an order of magnitude slower than seismic waves, their delay time with respect to seismic arrivals increases strongly with distance, being detected in the most remote stations about 16 hours after the moment of the explosion.

The detection in seismic data of air pressure changes due to the passage of cold fronts in is quite common and is attributed to the Newtonian attraction of the sensor mass by the change in density of the atmosphere above the instrument [8]. Figure 2a shows the signals related to atmospheric waves generated by the Hunga-Tonga eruption as recorded in the seismic station CAVN, part of the CA network [9] and located in NE Iberia, at about 17.600 km from the volcano. Although the signals can be identified in the three components of the seismic records, their amplitude is greater in the north-south oriented component, as this is the relative orientation between Tonga and NE Iberia. The spectrogram shows two arrivals about 4 hours apart, with spectral content restricted to the 1–3 mHz range (orange dashed lines in Fig. 2a). These arrivals correspond to Lamb waves that have traveled following the two directions of the great circle between the point of origin and the place of registration. Overprinting the first Lamb wave, the spectrogram shows the arrival of a wave with a strong dispersive character, with frequencies around 1 mHz arriving a few minutes after the Lamb wave and frequencies around 40 mHz arriving 45 minutes

later (line dashed red in Fig. 2a). Wright et al 2022 has shown the existence of gravity waves with continuously varying speeds that could correspond to our observations, although further modeling will be needed to assess this point. The dispersive wave corresponding to the long pathway is not observed, probably due to the effect of attenuation. The arrival of two atmospheric waves with differentiated spectral properties is observed in a large number of the stations analyzed.

Analysis of the extended time recordings up to 5 days (Fig. 2b) reveal further features. Seismic waves from the main blast arrive at this station 20 minutes after the time of origin (blue dashed line), while atmospheric waves propagating along the shortest path between Tonga and Iberia arrive 16 hours later. After large earthquakes, it is common to record multiple global circling waves, separated by intervals of close to 3 hours. In this case, what is recorded seismically is the passage of a Lamb wave traveling at acoustic speed and therefore taking around 36 hours to circumnavigate the planet. Clear signals around 10:00 on the 17 January and an additional one around 22:00 on the 18 January (Fig. 2b) are easily identified. This highlights the enormous energy generated by the main explosion, which has allowed its seismic detection after propagating for more than 100,000 kilometer during three and a half days. No dispersion is observed for the second and third passages of the atmospheric wave, suggesting that in these cases the recorded energy corresponds to a pure Lamb wave.

Although not all surveyed stations clearly show these arrivals, we have found that it is a fairly common observation. A four-day long representation of low-frequency seismic data (Fig. 3) reveal multiple passages of the Lamb wave, with stations located far from the source and its antipodal point detecting up to five Lamb wave passages. To our knowledge, there are no previous observations of this kind of long-lived atmospheric-ground coupling.

3 Low-frequency Near-monochromatic Signals

Figure 4 shows the seismic trace and the corresponding spectrogram for two stations located at different epicentral distances, POHA (Pohakuloa, Hawaii), at 4955 km, and PAB (San Pablo, central Spain) at 17735 km. In both cases, the arrival of the seismic waves generated by the volcanic explosion is shown with blue dashed lines. Red dashed lines show the Lamb waves, which reach POHA around 8:30 and PAB around 20:00. The most prominent feature of the spectrograms is the high energy detected around 3 mHz, lasting 10–12 hours.

This low-frequency, long-duration signal appears clearly in a seismic section similar to the one presented in Fig. 1, but now filtering between 2.5 and 6.5 mHz (Fig. 5a) shows a seismic section similar to the one presented in Fig. 1, but now filtering between 2.5 and 6.5 mHz. The first observations of this kind of signals date back to the early 1990s, following the eruption of Mount Pinatubo in 1991 [10,11]. The signals were described as a bichromatic, with two spectral peaks at 3.7 y. 4.3 mHz. Inspecting previous data, [11] identified similar signals produced by the 1982 El Chinchón eruption, with spectral peaks located in this case at 3.7 and 5.1 mHz. No further evidence of low-frequency seismic signals observed worldwide since then has been reported, but Dautermann et al. (2009) reported signals with a maximum amplitude of

around 4 mHz, after the collapse of the explosive lava dome. de Soufrière Hills (Montserrat, Lesser Antilles) in July 2003 km on borehole dilatometers measuring volumetric strain on Montserrat Island.

To better explore the properties of these signals, we have calculated the spectra of each seismic station using a 24 hours interval. The spectra obtained for a selection of sites, evidences the presence of clearly defined amplitude peaks between 3 and 6 mHz (Fig. 6). As the frequency and relative amplitude of these peaks are rather constant, we have stacked the results obtained from the 95 available stations to produce the stacked spectra shown as a blue line. The regular spacing of the peaks suggest that they may be related to the spheroidal normal modes of the Earth that form the so-called “Earth’s Hum”. To verify this point we have added to the figure the eigenfrequencies of the Earth, calculated from the PREM Earth reference model [13], as reproduced in [14]. As clearly shown, the dominant frequency is 3.7 mHz and corresponds to the oS29 spheroidal mode. A second group of spectral peaks with high energy is seen around 4.65 mHz. Moving to higher frequencies, a third group can be identified around 5.4 mHz and a last one around 6.0 mHz. It is interesting to note that for each of these groups, the modes around the dominant one also have significant energy.

Kanamori and Mori (1992) and Widmer and Zürn (1992) interpreted the two spectral peaks observed in their data as resulting from two atmospheric waves, the low frequency one being a gravity waves and the other a pressure wave.Widmer and Zürn 1992) pointed out a feedback regime between the atmosphere and the volcano and attributes the difference in the high frequency value between El Chinchón and Mount Pinatubo (5.1 vs 4.4 mHz) to temperature changes in the atmosphere affecting the pressure wave. Following a different approach,[15] considered the solid Earth and the atmosphere as a single system and calculated the theoretical normal modes, concluding that the 3.7 and 4.4 mHz nodes are the ones with the highest energy in the atmosphere. Using these theoretical modes, Lognonné (2009) built synthetic seismograms that fit the signals from Mount Pinatubo and showed, as in our dataset, a significant increase in amplitude near the antipodal point. The Mount Pinatubo model found reasonable amplitudes only for a source located at 24–28 km of altitude. Although it will be necessary to elaborate a specific synthetic model for the case of the Hunga-Tonga eruption, we would like to indicate that the twin waveforms separated by about 200 s observed for the events of 04:00 and 5:30 could be explained by a source located in this height range and a wave reflection at the top of the stratosphere.

The spectra stack constructed using 95 stations distributed around the world shows that the signal cannot be described as bichromatic, as there is a clearly dominant mode group around 3.7 mHz, but also three other mode groups with relatively high amplitudes, with maximums at 4.5, 5.3 and 6.0 mHz. For all four groups, the main mode has peaks of lower amplitude on both sides and that all of them coincide with the eigenfrequencies of the PREM Earth reference model. Thus, we favor an origin related to a coupling of the atmospheric system-solid Earth, in which the large atmospheric explosion resulted in the excitation of the normal modes of the Earth between 2 and 6 mHz, the so-called “Earth's Hum”, with higher amplitudes at frequencies where atmospheric waves carry more energy and can be better transferred to the ground.

As seen in Fig. 5b, at stations located at large epicentral distances, the amplitude of the low-frequency signal decreases smoothly with time, only to increase again between 09:00 and 10:00 UTC. The timing of this increase coincides with the arrival of surface seismic waves generated by the 08:30 volcanic explosion (see section 2), which suggests that this event may have increased the level of normal mode excitation, a hypothesis that should be confirmed by future modelling.

4 Concluding Remarks

Analysis of seismic data collected by networks on a global scale has provided new information regarding the temporal evolution of the Hunga-Tonga eruption, confirming that the three umbrella clouds identified in the satellite data at 04:00, 05:30 and 08:30 are associated with strong explosions that have generated seismic waves propagated on a global scale. The main eruption started a few minutes before the time indicated in the seismic catalogs and had a complex waveform that includes two energy packets separated by 200 to 210 s. The 05:30 event shares a similar waveform, suggesting that the second packet could in fact be an atmospheric reflection of the wave generated by the main explosion.

The atmospheric Lamb wave has been detected in seismometers during 3 and a half days, with many sensors detecting up to five passages of the wave, hence evidencing the exceptional energy liberated by the Hunga-Tonga explosion. During the first passage, many seismic stations show the arrival of a second atmospheric wave, of a dispersive nature, that moves with a slightly lower speed, which could correspond to a gravity or pressure wave.

The low-frequency and long-duration signals identified in this episode had only been previously described as a consequence of the 1982 El Chinchón and 1991 Mount Pinatubo volcanic eruptions, and should be considered exceptional. Observed at a large number of sites distributed around the world, these signals are attributed to the excitation of the Earth's normal modes as a consequence of the main volcanic explosion. Considering that the normal mode with more energy is 3.7 mHz, we can say that the Earth has been beating every 4.5 minutes during the hours following the powerful Hunga-Tonga explosion.

Methods

To inspect the seismic data at global scale, we have selected a group of broad-band seismic stations integrated in the main worldwide-scale seismic networks, including the Global Seismograph Network [17], the IRIS/IDA seismic network [18], Geoscope[19] and Geofon [20]. We have downloaded and processed the available data, restricting ourselves to the LHZ channels, with a sampling rate of 1 sample per second. In addition, we have inspected data from the broad-band seismic networks covering SW Europe, including the FR [21], ES[22] and CA[9] networks to check eventual regional scale variations in an area not far from the antipodal position with respect to the eruptive zone.

The instrument response has been removed from the data using the standard procedures included in the Obspy package (ref).

Spectra and spectrograms are calculated using SAC and Obspy routines.

Declarations

Acknowledgements

I want to acknowledge all the teams involved in the design, installation and maintenance of broadband seismic networks around the world, which provide the essential data to carry out these type of studies. I also want to thank ORFEUS EIDA (http://www.orfeus-eu.org/data/eida/) and FDSN (https://www.fdsn.org/services/) data services for providing easy access to seismic data. The manuscript has been enriched by fruitful discussions with different colleagues, and in particular with Drs. M. Ruiz and M. Schimmel. This work has been benefited from the infrastructure of the GEO3BCN-CSIC (Labsis) seismic laboratory.

References

1. Garvin, J. Dramatic Changes at Hunga Tonga-Hunga Ha‘apai. https://earthobservatory.nasa.gov/images/149367/dramatic-changes-at-hungatonga- hunga-haapai (2022).
2. Carr, J. L., Horvath, A., Wu, D. L. & Friberg, M. D. Stereo Plume Height and Motion Retrievals for the Record-Setting Hunga Tonga-Hunga Ha’apai Eruption of 15 January 2022. Earth and Space Science Open Archive 10 (2022) doi:10.1002/essoar.10510365.1.
3. Zhang, S.-R. *et al.* 2022 Tonga Volcanic Eruption Induced Global Propagation of Ionospheric Disturbances via Lamb Waves. Frontiers in Astronomy and Space Sciences **9**, (2022).
4. Themens, D. R. *et al.* Global propagation of ionospheric disturbances associated with the 2022 Tonga Volcanic Eruption. Geophysical Research Letters (2022) doi:10.1029/2022GL098158.
5. Yuen, D. A. *et al.* Under the Surface: Pressure-Induced Planetary-Scale Waves, Volcanic Lightning, and Gaseous Clouds Caused by the Submarine Eruption of Hunga Tonga-Hunga Ha’apai Volcano Provide an Excellent Research Opportunity. Earthquake Research Advances 100134 (2022) doi:10.1016/j.eqrea.2022.100134.
6. Amores, A. *et al.* Numerical Simulation of Atmospheric Lamb Waves Generated by the 2022 Hunga-Tonga Volcanic Eruption. Geophysical Research Letters **49**, (2022).
7. Kumar Gupta, A., Bennartz, R., Fauria, K. E. & Mittal, T. Timelines of plume characteristics of the Hunga Tonga-Hunga Ha’apai. (2022) doi:10.1002/essoar.10510853.1.
8. Zürn, W. & Widmer, R. On noise reduction in vertical seismic records below 2 mHz using local barometric pressure. **22**, (1995).
9. Institut Cartogràfic i Geològic de Catalunya. Catalan Seismic Network. International Federation of Digital Seismograph Networks. Other/Seismic Network. (2000) doi:10.7914/SN/CA.

10. Kanamori, H. & Mori, J. Harmonic excitation of mantle Rayleigh waves by the 1991 eruption of Mount Pinatubo, Philippines. Geophysical Research Letters **19**, 721–724 (1992).
11. Widmer, R. & Zürn, W. Bichromatic excitation of long-period Rayleigh and air waves by the Mount Pinatubo and El Chinchón volcanic eruptions. Geophysical Research Letters **19**, 765–768 (1992).
12. Dautermann, T., Calais, E., Lognonné, P. & Mattioli, G. S. Lithosphere-atmosphere-ionosphere coupling after the 2003 explosive eruption of the Soufriere Hills Volcano, Montserrat. Geophysical Journal International **179**, 1537–1546 (2009).
13. Dziewonski, A. M. & Anderson, D. L. Preliminary reference Earth model. Physics of the Earth and Planetary Interiors **25**, 297–356 (1981).
14. Tanimoto, T., Heki, K. & Artru-Lambin, J. Interaction of Solid Earth, Atmosphere, and Ionosphere. in *Treatise on Geophysics: Second Edition* vol. 4 421–443 (Elsevier Inc., 2015).
15. Lognonné, P., Clévédé, E. & Kanamori, H. Computation of seismograms and atmospheric oscillations by normal-mode summation for a spherical earth model with realistic atmosphere. Geophysical Journal International **135**, 388–406 (1998).
16. Lognonné, P. Seismic waves from atmospheric sources and atmospheric/ionospheric signatures of seismic waves. in *Infrasound Monitoring for Atmospheric Studies* 281–304 (Springer Netherlands, 2009). doi:10.1007/978-1-4020-9508-5_10.
17. Albuquerque Seismological Laboratory & USGS. Global Seismograph Network - IRIS/USGS. International Federation of Digital Seismograph Networks. Dataset/Seismic Network. (1988) doi:10.7914/SN/IU.
18. Scripps Institution of Oceanography. Global Seismograph Network - IRIS/IDA. International Federation of Digital Seismograph Networks. Dataset/Seismic Network. (1996) doi:10.7914/SN/II.
19. Institut de Physique du Globe de Paris & Ecole et Observatoire des Sciences de la Terre de Strasbourg. GEOSCOPE, French Global Network of broad band seismic stations. (1982) doi:10.18715/GEOSCOPE.G.
20. GEOFON Data Centre. GEOFON Seismic Network. Deutsches GeoForschungsZentrum GFZ. (1993) doi:10.14470/TR560404.
21. RESIF. RESIF-RLBP French Broad-band network, RESIF-RAP strong motion network and other seismic stations in metropolitan France [Data set]. RESIF - Réseau Sismologique et géodésique Français. (1995) doi:10.15778/RESIF.FR.
22. Instituto Geografico Nacional, S. Spanish Digital Seismic Network [Data set]. International Federation of Digital Seismograph Networks. (1999) doi:10.7914/SN/ES.

Figures

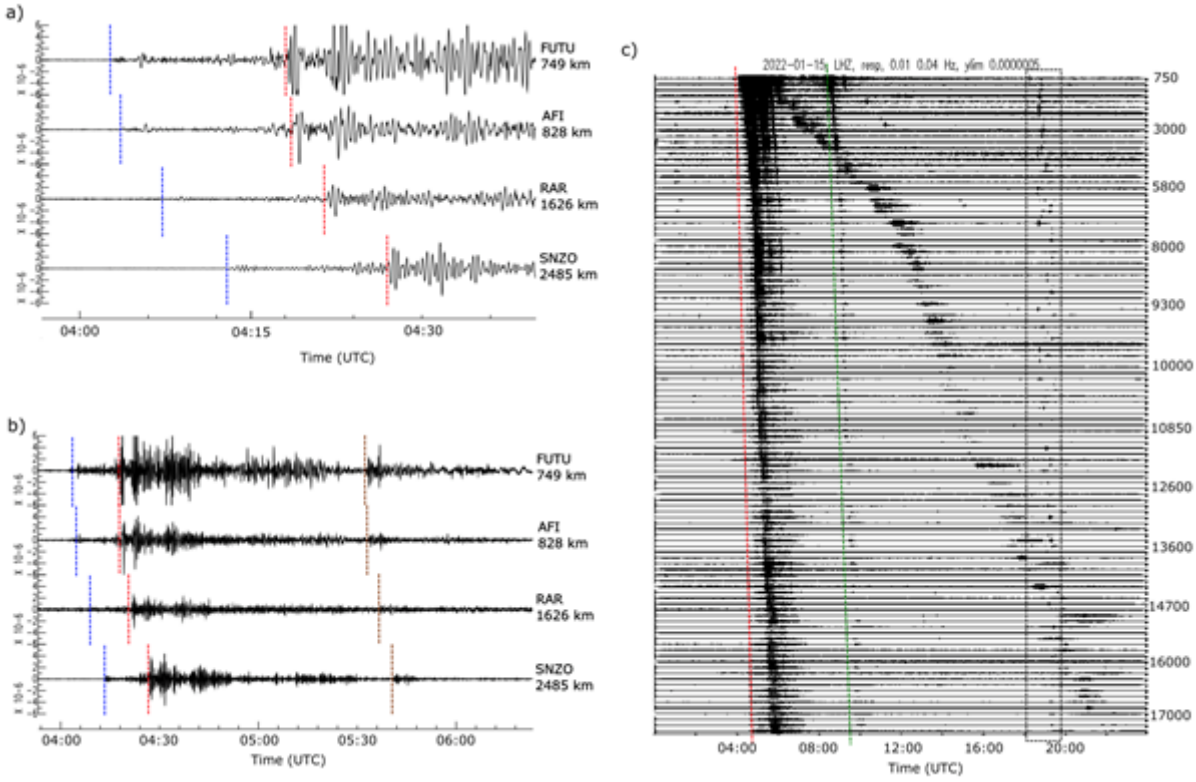

Figure 1

Seismic records of the Hunga-Tonga eruption. Instrumental response has been removed, data has been filtered between 0.01 and 0.04 Hz and plotted without amplitude normalization. The amplitudes of the signals are expressed in m/s and the traces are ordered according to their epicentral distance. a) Detail of the signal onset at the closest stations. Red dashed line shows the most energetic arrival, compatible with the origin time in seismic catalogs. Blue dashed line shows the first arrival observed in the filtered data. The labels indicate the name of the station and the distance to the origin. b) Larger-scale scale view of the same dataset, showing the arrival from a second event detected around 05:30 (brown dashed lines) c) Seismic traces for the entire dataset during January 15, 2022. Red line shows the main arrival and green line the phases related to the event detected around 08:35. The black box shows the arrivals from a 5.7 magnitude earthquake with epicenter in the Pacific-Indian Ridge. The signal observed in intermediate times propagating with slow.

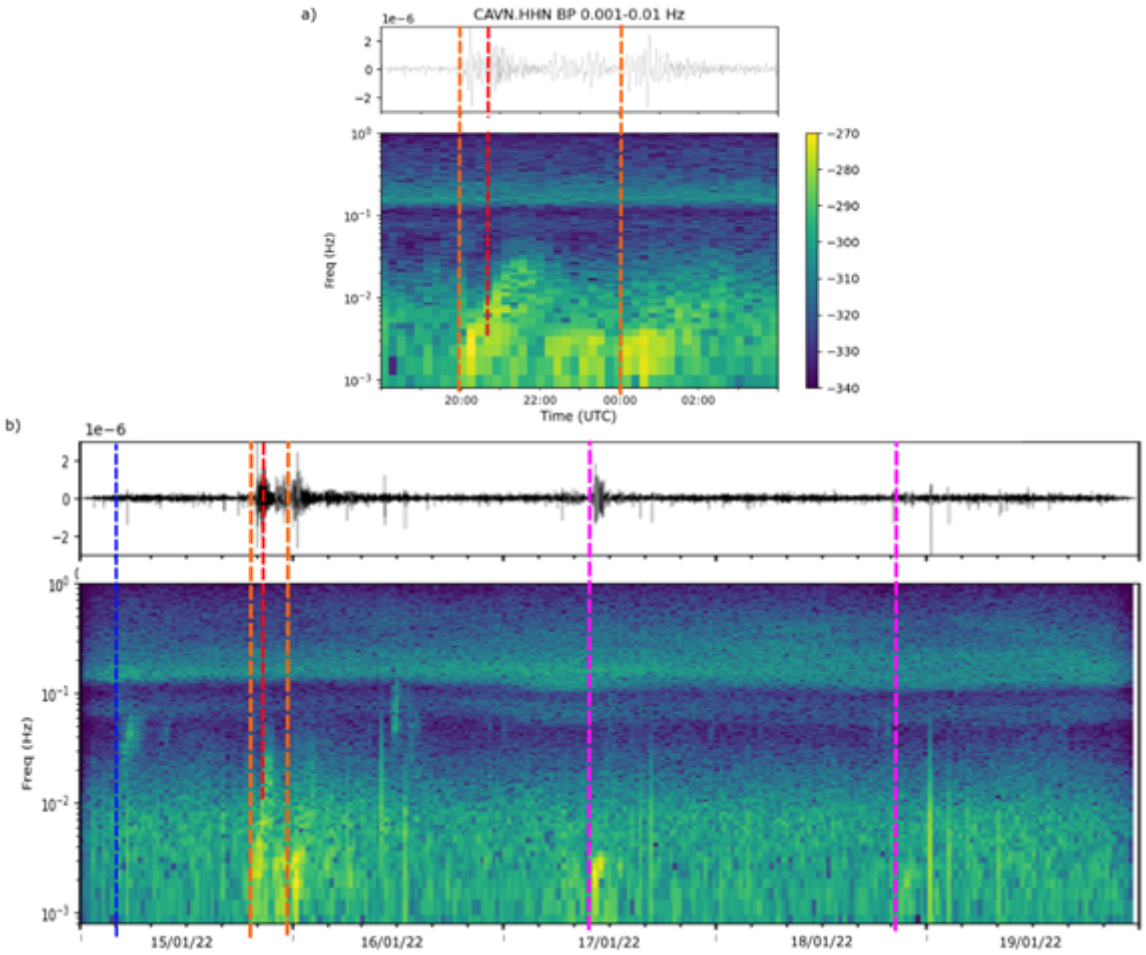

Figure 2

a) Arrival of the atmospheric wave to station CA.CAVN, located in NE Iberia (NS component). The instrument response has been removed and the seismic trace has been band-pass filtered between 1and 10 mHz. The spectrogram corresponds to the unfiltered data and was calculated using a window length of 1800s. Orange lines show the arrival of the Lamb waves traveling along the short and long path of the great circle. Red dashed line shows the arrival of the dispersive wave. b)5 days of seismic signal and spectrogram at the same station. Blue dashed line shows the arrival of the seismic waves. Orange and red dashed lines show the first arrivals of the atmospheric waves. Purple lines shows the record of the atmospheric waves after successive circumambulations of the Earth.

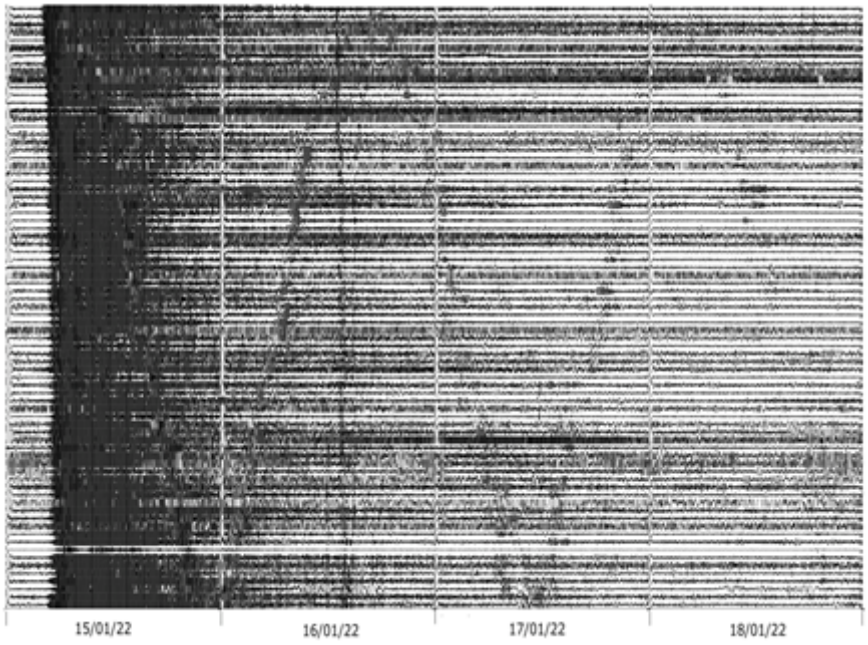

Figure 3

Seismic record of the successive passages of the atmospheric Lamb wave in stations distributed throughout the planet. The data have been band-pass filtered between 0.5 and 5 mHz, classified according to their distance from Hunga-Tonga and represented without amplitude normalization.

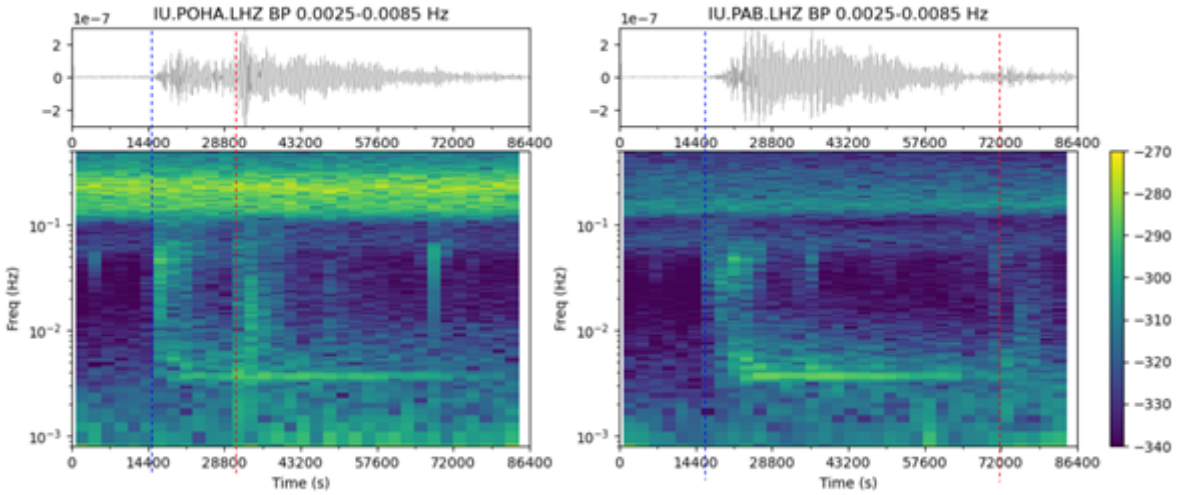

Figure 4

a) Seismic traces and spectrograms for two representative sites; IU.POHA station, located in Hawaii, and IU.PAB, located in central Spain. The traces have been corrected for the instrument response and filtered between 2.5 and 6.5 mHz. Amplitudes are expressed in m/s. Blue dashed lines show the onset of the low-frequency signal, while red dashed lines show the arrival of the Lamb waves.

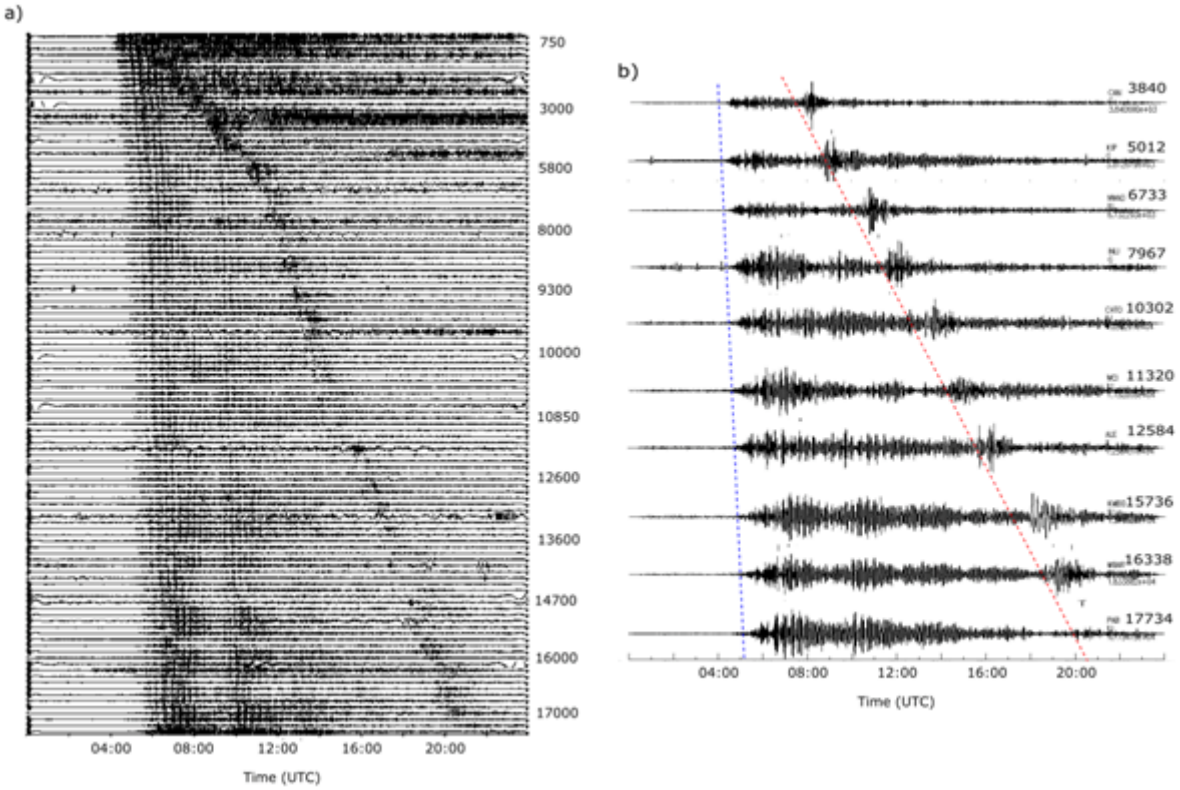

Figure 5

a) Seismic traces for the entire dataset filtered between 2.5 and 6.5 mHz. The instrument response has been removed and the traces are not normalized in amplitude. Labels show the distance to the Hunga-Tonga volcano (in km). b) Selected traces at different distance ranges, filtered in the same frequency band. Blue dashed line marks the onset of the low-frequency signal and red dashed lines mark the arrival of the atmospheric Lamb waves.

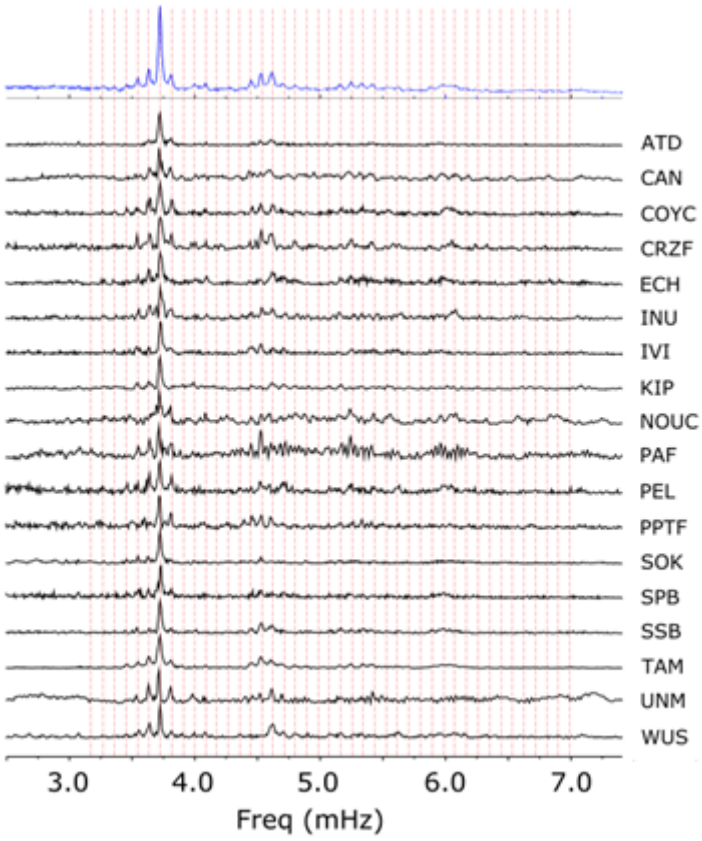

Figure 6

Normalized amplitude spectra for a selection seismic stations distributed throughout the world (Geoscope network), calculated for the 24 hours of the day of the eruption. Blue line shows the spectra stack of the 95 traces analyzed. Red dashed lines show the eigenfrequencies for the PREM model.